Simulating the Induction Heating Behavior of CFRTPC Laminates

Thomas Hoffmann, Stephan Becker, Miro Duhovic, Peter Mitschang

Leibniz-Institut für Verbundwerkstoffe GmbH, Technische Universität Kaiserslautern, Erwin-Schrödinger-Straße 58, 67663 Kaiserslautern, Germany

Abstract

The objective of this work is to create an FEM-based model for the inductive heating of carbon fiber reinforced thermoplastic composite (CFRTPC) laminates. A macroscale simulation model was created using the multi-physics capabilities of LS-DYNA®. Material model parameters were largely determined by micromechanical considerations. In order to further increase the accuracy of the FEM model, dynamic differential calorimetry (DSC) measurements were also carried out to determine the temperature dependence of the heat capacity of the laminates investigated. The model was then validated for laminates reinforced by non-crimped fabrics (NCF) with fiber volume contents (FVC) of 32%, 47% and 60% via induction heating tests. In general, the heating experiments could be approximated well both qualitatively and quantitatively. Furthermore, analyses were carried out in order to investigate the influence of individual ply orientations in the laminate on one another as well as the influence of the layer thickness on the resulting heating behavior.

1 Introduction

In the goal towards zero-emission aircraft design, weight efficiency is the decisive parameter. In combination with the challenges of new fuel storage systems and improved aircraft aerodynamics, novel aircraft geometries play a key role. A particular challenge is the shift from cylindrical fuselage designs to complexly curved structures utilizing integral, thermoplastic part design and manufacturing methodologies as well as the connection of these parts with one another. The continuous induction welding method fits well into this requirement profile due to its high degree of automation and energy efficiency. In addition, next generation manufacturing and computer aided engineering (CAE) technologies for the design of CFRTPC induction welding/joining processes for commercial aircraft structures also play a pivotal role. Modeling the induction heating process not only serves to optimize laminate structures with respect to heating behavior, but also represents an important step towards designing efficient process control.

1.1 Inductive heating of carbon fiber reinforced thermoplastic composites

The induction welding process considered in this paper belongs to the category of electromagnetic based welding processes, which can be further categorized into discontinuous and continuous induction welding [1]. The principle of the process is based on induction heating, which relies on the induction of eddy currents within the laminate by a current-carrying coil (Figure 1).
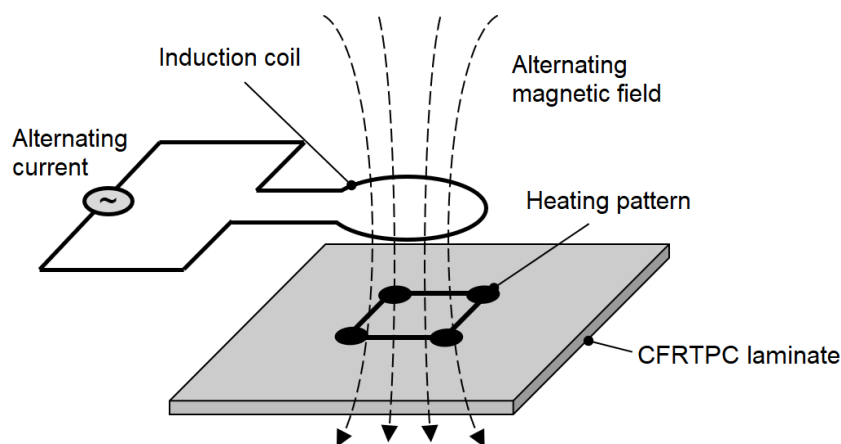

Fig.1:   Setup for induction heating of CFRTPC laminates according to [2].

The eddy currents cause an intrinsic heating in the material to be welded. A prerequisite for the occurrence of such eddy currents is sufficient electrical conductivity of the material. Since polymers have electrically insulating properties, electrically conductive fibers (e.g. carbon fibers) must be used. To ensure the formation of electrically conductive loops in the material, the CFRTPC must also have sufficient electrical conductivity in all directions. Therefore, CFRTPCs with unidirectional (UD) fibers are in principle unsuitable for induction heating. However, quasi-isotropic laminates and fabrics due to their resulting fiber structures are well suited. As an alternative to conductive fibers, metallic susceptors can also be used to generate the heat required within the joining zone [2].

1.1.1 Heating mechanisms of induction heating of CFRTPCs.

Induction heating of CFRTPCs is mainly based on three heating mechanisms. The influence of these heating mechanisms is significantly influenced by the type of laminate used. The basis of the heating mechanisms is always the physical effect that power losses occur due to electrical resistances or impedances, which are then expressed in terms of heat generation. A distinction can be made between Joule losses, dielectric losses and contact losses (Figure 2 a). Since the electric current always chooses the path of least resistance, it preferentially runs along the length of the carbon fibers and is therefore bound to their orientation. The electrical resistance of the fibers causes the Joule heating losses. In order for current loops to form, the current must switch direction. This occurs at the crossover points of the rovings (Figure 2 b). The losses occurring here can be further differentiated by contact losses and dielectric losses [3].
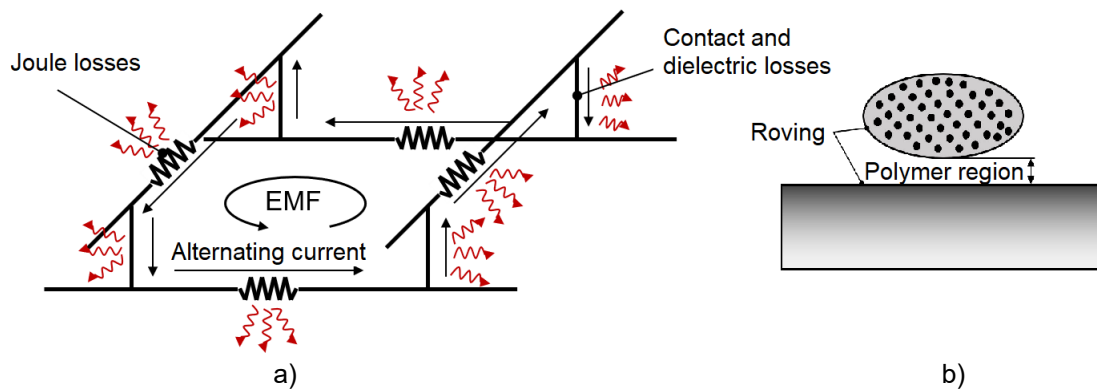

| | a) | b) |

Fig.2: a) Model of a conductor loop with the joule, contact and dielectric losses according to [3] and b) the polymer region in which dielectric losses occur according to [4].

2 Materials

In order to validate the model created in this work, induction heating experiments have been carried out. Three different non-crimped fabric (NCF) laminates have been used for the validation tests as listed in Table 1. The laminates consist of three different fiber volume fractions (32%, 47% and 60%). For manufacturing reasons, the thicknesses of the different laminate structures differ. The polymer used is PA66.

	PA66 NCF 32%	PA 66 NCF 47%	PA66 NCF 60%
Textile structure	NCF	NCF	NCF
Fiber	CF	CF	CF
Matrix	PA66	PA66	PA66
Fiber volume fraction (V_f)	32 %	47%	60%
Number of layers	6	9	12
Layup configuration	-45°/+45°	-45°/+45°	-45°/+45°
Laminate thickness	≈ 2.2 mm	≈ 2.0 mm	≈ 2.5 mm

Table 1: Overview of laminates used in heating experiments

3 Creation of the FE model

3.1 Geometry

The model created in this work is limited to the inductor and a small section of the laminate. The laminate has a square base with a side length of 100 mm. The thickness of the laminate t_{Lam} is variable and depends on the number of layers in the laminate. The inductor is located centrally at a distance of 5 mm (inductor bottom to laminate top) above the laminate, as shown in Figure 3 a). In this test case, the inductor remains stationary. Therefore, only the static heating behavior of the laminate is determined, which allows a comparison with the static heating tests for validating the model.
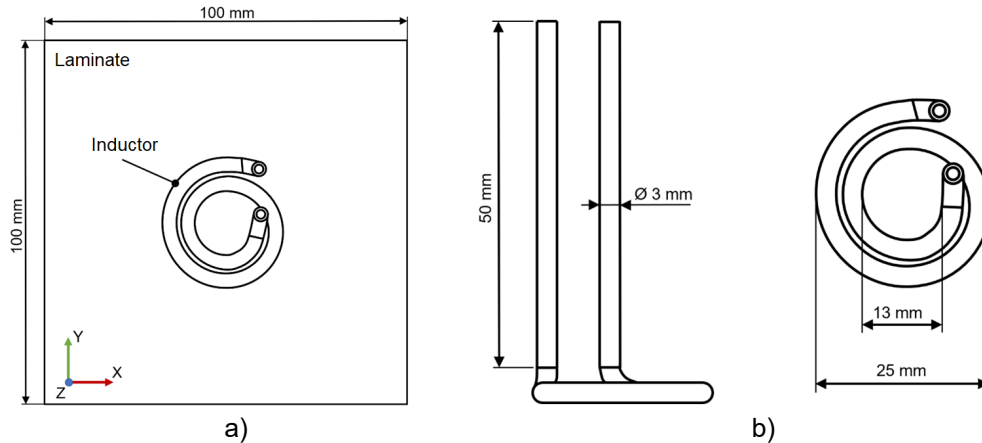

Fig.3:   Schematic representation of a) the complete FE model and b) the induction coil geometries.

The inductor is a pancake coil with an outer diameter of 25 mm and has two windings. All other relevant dimensions are shown in Figure 3 b).

3.2 Material model

In addition to the structure of the FE model, the material model also has a major influence on the accuracy of the results. For this reason, particular care must be taken to ensure that the assumptions and simplifications made do not have a major influence on the material behavior in the simulation. The material model created in this work is based on an analytical model developed at the Institut für Verbundwerkstoffe (IVW). The analytical model itself is based on the electrical circuit shown in Figure 4 b. The model considers and distinguishes between three different heating mechanisms:

- R_f stands for the resistance of the individual fibers and thus for the Joule losses which occur in the fibers. The heat generation due to the Joule losses can be calculated via I_{total}, the total current and U_f, the voltage drop across the fibers.
- R_{jc} stands for the crossover losses which occur when the current switches to a roving of a different fiber orientation. This can be further subdivided (Figure 4 a) to include the dielectric losses.
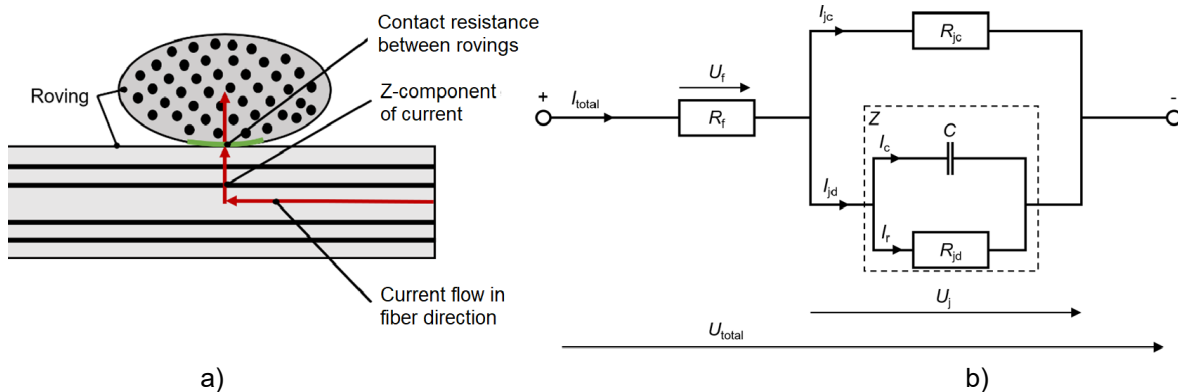- The system Z therefore represents the impedance created by the dielectric behavior of the matrix.

Fig.4:   Schematic representation of a) the current flow when changing the fiber orientation and b) its representative electrical circuit.

Over the further course of investigations carried out at the IVW, it was shown that the heat generation resulting from the dielectric behavior is negligible. Therefore, the model can be further simplified by connecting R_f and R_{jc} in series. A wide range of modeling approaches are possible for the FEM simulation of induction heating of CFRTPCs. The distinction between the micro, inter, meso and macro levels is shown schematically in Figure 5 and take place at different geometric scales. The material model created in this work can be assigned to the mesoscopic level. Therefore, the influence of the layer thicknesses and also the stacking sequence of the individual layers in the laminate on the heating behavior can be considered with reasonable calculation time. Furthermore, the crossover losses can be modeled directly via the thickness resistances of the laminate. An extension of the model to include contact resistances between the layers is also made possible by the use of a mesoscopic approach. The thickness resistance of the laminate as well as the contact resistances between the rovings can therefore be modeled discretely.
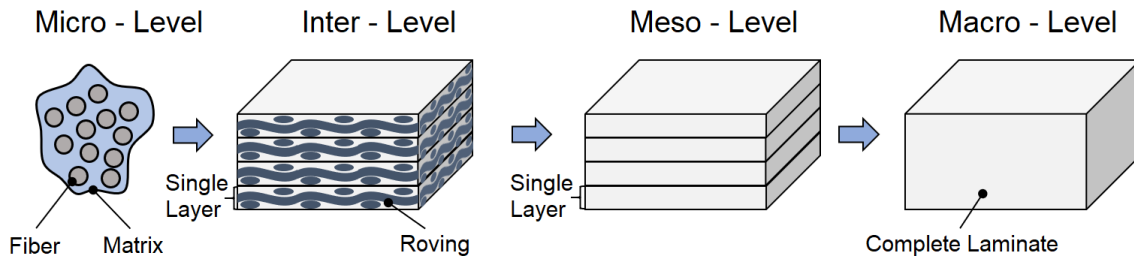

Fig.5: *Different levels of material homogenization considered for the FE modeling of CFRTPCs [5].*

A summary of the simplifications and assumptions that have been made for the meso-level laminate model are outlined as follows:

- The laminate is composed of several ideal homogeneous UD-layers. In NCF laminates, each UD-layer represents a fabric ply. For fabric laminates, a UD layer in 0° ply represents the fibers in the warp direction. The weft direction is represented by a layer in 90° direction.
- The fibers lie parallel to each other and are evenly distributed throughout the UD layer.
- The tangential as well as radial thermal conductivity of the fibers are identical.
- The thermal conductivities of the UD-layer are independent of temperature.
- The fiber-dominated electrical conductivities of the UD-layer are independent of temperature.
- The electrical conductivity of the UD-layer in the fiber direction depends only on the V_f of the layer. The matrix used does not play a significant role due to the electrically insulating properties and thus low conductivity values.
- All material properties of the inductor are also considered independent of temperature.

Consequently, all parameters collected for the simulation refer to the UD-layer.

3.2.1 Electrical properties of the laminates and the inductor

The material model created in this work is based on the analytical approach presented in the previous section. After the simplification and the omission of the dielectric losses, R_f and R_{jc} must therefore be implemented into the FE model in order to represent all relevant parts of the analytical model.

For the electrical properties of a UD-layer and the inductor, the following parameters are therefore required:

- Electrical conductivities parallel and transverse to the fiber direction of the UD-layer $\sigma_\parallel$ and $\sigma_\perp$. The conductivity value $\sigma_\parallel$ takes the role of R_f from the analytical model. $\sigma_\perp$ takes the role of the resistance R_{jc}.
- Magnetic permeability μ of the laminate
- The electrical conductivity of the copper inductor σ_{Copper}

Within the electromagnetic material models available in LS-DYNA®, the electrical conductivities of a UD-layer can be described by a second order tensor (see Table 3). Conductivities of the individual layers in the fiber direction are determined via a parallel connection of fiber- and matrix conductivities. Since the electrical conductivities of PA66 are very low compared to carbon fiber, they are assumed to be negligible [6]. The electrical conductivities of the fiber are taken from the literature [7]. The electrical conductivity of the UD-layer perpendicular to the fiber direction is also taken from the literature [8]. Since these conductivities are applied numerically to create entire CFRTPC-laminates and include contact losses, discrete modeling of the resistance R_{jc} is not necessary. Therefore, the electrical conductivity tensor of the UD-layer depends only on the fiber volume fraction V_f. For the electrical conductivity of the copper inductor, a literature value is used [9]. A summary of the electrical conductivity values used is given in Table 2.

The inductor as well as the laminate are both surrounded by air. The use of air as a surrounding medium can be defined directly in LS-DYNA®. Further definition of the electromagnetic or thermal properties of the air is not necessary. As mentioned before, all electrical material properties are assumed temperature independent. Therefore, when the temperature of the laminate or the inductor changes, no change in the magnetic field is considered. Therefore, in the simulation of the validation tests the magnetic field only has to be calculated only once at the beginning of the simulation.

V_f	32%	47%	50%	60%	Inductor
Electrical conductivity in S/m	$\begin{bmatrix} 16000 & 0 & 0 \\ 0 & 0,03 & 0 \\ 0 & 0 & 0,03 \end{bmatrix}$	$\begin{bmatrix} 23750 & 0 & 0 \\ 0 & 0,6 & 0 \\ 0 & 0 & 0,6 \end{bmatrix}$	$\begin{bmatrix} 25000 & 0 & 0 \\ 0 & 1 & 0 \\ 0 & 0 & 1 \end{bmatrix}$	$\begin{bmatrix} 30000 & 0 & 0 \\ 0 & 10 & 0 \\ 0 & 0 & 10 \end{bmatrix}$	$6 \cdot 10^7$

Table 2: Overview of the calculated electrical properties of the UD-layers at different fiber volume contents and the inductor coil.

3.2.2 Thermal properties of the laminates and the inductor

For the description of the thermal behavior of the laminate and the inductor, the following material parameters are necessary:

- Thermal conductivities of inductor and UD-layer parallel and transverse to fiber direction $\lambda\|$, $\lambda\perp$
- Heat capacity, c of the inductor and UD-layer
- Density, ρ of inductor and UD-layer
- Melting temperature, T_m of PA66
- Melting enthalpy of the UD-layer

The thermal conductivities $\lambda\|$ and $\lambda\perp$ of the UD-layer are both determined via micromechanical approaches (parallel- ($\lambda\|$) and series-connection ($\lambda\perp$) of thermal conductivities of the fiber and matrix constituent properties) (Table 3) [7]. The density of the laminate is determined via the rule of mixtures. The heat capacity of PA66 cannot be assumed to be constant for the temperature range considered. Furthermore, the heat capacity used in the simulation has a direct influence on the heating rate. The heat capacity given in literature as well as on data sheets of the manufacturers is mostly limited to a value for room temperature. Therefore, the heat capacity of PA66 was measured by means of DSC.
Since all UD-layers in a laminate have the same V_f, it can be assumed that the heat capacity of a UD-layer and a laminate are identical. The heat capacity measurement is carried out on unreinforced PA66 grade Ultramid® A4H [10]. The heat capacity of the UD-layer is then calculated for the different fiber volume fractions (32%, 47%, 50%, 60%) using the rule of mixtures based on the measured heat capacity determined for pure PA66. The heat capacity of the carbon fibers is assumed to be constant within the temperature range considered.

The heat capacities of the UD-layers are entered into LS-DYNA® as six value pairs via the ***MAT_THERMAL_ORTHOTROPIC_TD** keyword. If necessary, ***MAT_THERMAL_ORTHOTROPIC_TD_LC** could also be used, however, in this case the shape of the heat capacity curve can be well represented with six value pairs. The heat capacity values used for the different fiber volume fractions in the simulation are given in Table 4. The respective enthalpies of fusion separated from the measured curve are indicated separately.

V_f	$V_f = 32\%$	$V_f = 47\%$	$V_f = 50\%$	$V_f = 60\%$	Inductor
Heat capacity in J/g·°C	Loadcurve (See table 5)	Loadcurve (See table 5)	Loadcurve (See table 5)	Loadcurve (See table 5)	0.382
Thermal conductivity in W/m·°C	$\begin{bmatrix} 1.72 & 0 & 0 \\ 0 & 0.32 & 0 \\ 0 & 0 & 0.32 \end{bmatrix}$	$\begin{bmatrix} 2.45 & 0 & 0 \\ 0 & 0.39 & 0 \\ 0 & 0 & 0.39 \end{bmatrix}$	$\begin{bmatrix} 2.57 & 0 & 0 \\ 0 & 0.4 & 0 \\ 0 & 0 & 0.4 \end{bmatrix}$	$\begin{bmatrix} 3.03 & 0 & 0 \\ 0 & 0.48 & 0 \\ 0 & 0 & 0.48 \end{bmatrix}$	390
Melt temperature in °C [10]	260	260	260	260	-
Melt Enthalpy in J/g	51.74	37.89	35.89	27.83	-
Density in kg/m³	1448	1514	1525	1568	8960

Table 3: Thermal properties of the inductor and the UD-layers at different V_f.

T in °C	$V_f = 32\%$	$V_f = 47\%$	$V_f = 50\%$	$V_f = 60\%$
		c in J/g·°C		
0	1.06	0.96	0.95	0.90
50	1.31	1.15	1.12	1.03
190	2.06	1.70	1.65	1.44
235	2.10	1.73	1.67	1.46
295	1.96	1.63	1.58	1.38
		c_{LAT} in J/g		
260	51.74	37.98	35.89	27.83

Table 4: Heat capacities and corresponding enthalpies of fusion used for the simulation at different V_f.

3.3 Boundary conditions of the FE model

Another important aspect of the FE model are the boundary conditions. For the simulation model created in this work, the electromagnetic and thermal boundary conditions required are summarized in Figure 6.
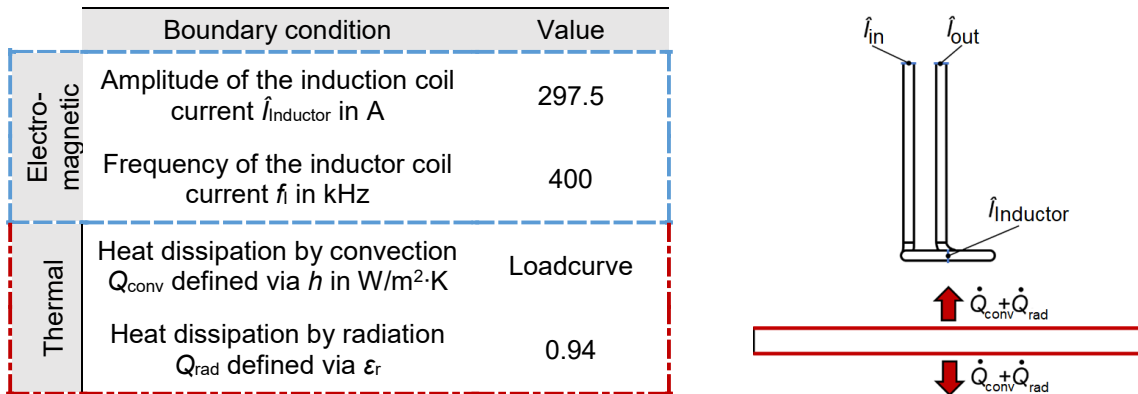
	Boundary condition	Value
Electro-magnetic	Amplitude of the induction coil current $\hat{I}_{Inductor}$ in A	297.5
Electro-magnetic	Frequency of the inductor coil current f_i in kHz	400
Thermal	Heat dissipation by convection Q_{conv} defined via h in W/m²·K	Loadcurve
Thermal	Heat dissipation by radiation Q_{rad} defined via ε_r	0.94

Fig.6: Overview and schematic representation of the electromagnetic (blue) and thermal (red) boundary conditions defined in the LS-DYNA® FE model.

3.3.1 Electromagnetic boundary conditions

To simulate the inductive heating of the laminate, the alternating current flowing through the inductor must be defined. This is done via electromagnetic boundary conditions. The amplitude of the current flowing through the inductor and its frequency at the two end faces of the coil are defined.

3.3.2 Thermal boundary conditions

The thermal behavior of the laminate has a decisive influence on the heating behavior during induction heating. Furthermore, the interactions of the laminate with the ambient air also play a role. In the model created, thermal boundary conditions are defined for free convection and thermal radiation at the top and bottom of the laminate. As the inductor is water-cooled and remains at a relatively constant temperature close to room temperature, no temperature-dependent material behavior needs to be defined. Therefore, no thermal boundary conditions are necessary for the inductor. If the exact

temperature of the coil is of interest, then a heat transfer coefficient could be defined on the inner surface of the coil to simulate the water-cooling effect.

3.4 Mesh convergence study

To enable FE analysis, the individual components of the model are meshed. For the laminate, only hexahedral elements are used which is a requirement of the solver in LS-DYNA®. Furthermore, a mesh convergence study was performed with the goal of reducing the computation time while ensuring accuracy of the results. Especially at locations of high magnetic field and temperature gradients, the mesh must have sufficient density to resolve local temperature increases accurately. Since the laminate used is still a very simple and small geometry, only h-adaptivity is used. This means that only elements of the same size are used for the laminate. The influence of the number of elements is considered independently in both the thickness and in the in-plane (x/y) directions of the laminate. The parameters used for the mesh convergence study are summarized in Table 5.

Parameter	Value
$\hat{I}$ in A	315.7
f in kHz	520
φ in %	47
t_{LAM} in mm	2.3
Layer configuration	$(0/90)_{10}$
Stop criteria (simulation time) in sec	5

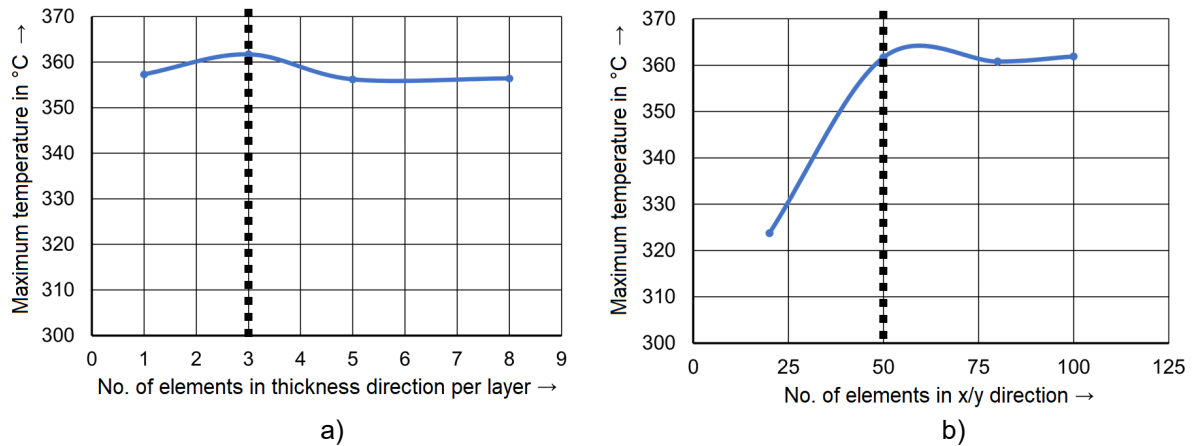*Table 5: Parameters used in the simulations for the mesh convergence analysis.*

Fig.7: Influence of the number of elements in the thickness direction per UD- ply a) and elements in-plane of the laminate b) on the maximum temperature developed in the laminate.
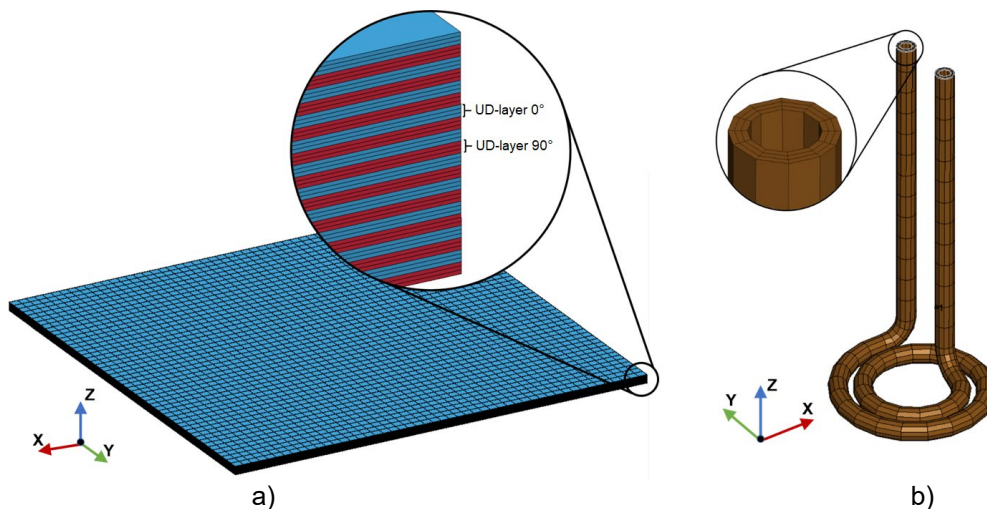

Fig.8: Mesh geometry of a) the laminate using the example of a 20-ply 0/90 NCF laminate. Each UD ply has three elements in the thickness direction and 50 elements in the X and Y direction and b) the pancake coil inductor

If the number of elements per UD-layer is varied in the thickness direction, it can be seen that even one element per layer is sufficient to determine the heating behavior of the laminate with sufficient accuracy (see Figure 7). However, if the current distribution in the laminate is considered, it can be seen that this only converges when using three elements or more per layer. If the number of elements in-plane is varied, it can be seen that the maximum temperature in the laminate converges with a resolution of 50 x 50 elements (2 mm element size) in the laminate. The subsequent simulations performed in this work are all carried out with 3 elements per UD-layer in the thickness direction and 50 x 50 elements in the in-plane direction of the laminate (see Figure 8). This ensures a sufficiently accurate calculation of the heating behavior. Furthermore, the current density distribution in the laminate can also be investigated with three elements in the thickness direction.

The model of the induction coil has already been used in other publications by the authors [11, 12, 13, 14] for similar applications in LS-DYNA® (see Figure 8 b) and is considered a high enough resolution to capture the shape of the magnetic field, therefore no further optimization of the mesh is necessary. For the inductor, hexahedral elements are required. The BEM method is used to model the surrounding medium between the laminate and the inductor. Therefore, no separate meshing of the air volume is necessary. The BEM matrix is automatically created by the EM solver at the start of the simulation.

4 Induction heating simulation

4.1 Validation of the FE model

The FE model created in this work is validated via heating tests. The laminates and their properties introduced in section 2 are used for both the simulation and the heating experiments. The material properties used for the simulation are derived from the methods described in section 3.2. In addition to the heating behavior of the different laminates, the influence of the layer configuration (orientation of the individual layers) on the heating behavior is also investigated for validation purposes.

4.1.1 Experimental setup of the validation tests

In order to validate the results of the simulation, heating experiments are carried out. The aim of these validation tests is to prove the validity of the FE model. For this purpose, simulation and test are qualitatively and quantitatively compared. The heating tests are carried out with an induction generator of the type "Power Cube PW3-32/400" from LTB Bachofer GmbH. The resulting heating of the laminate is measured on the side facing the inductor as well as on the opposite side with two thermal imaging cameras of the type TIM 160 from Micro Epsilon Messtechnik GmbH. The evaluation of the video data is carried out with the software "TIM Connect" from Micro Epsilon Messtechnik GmbH. The underside of the pancake inductor used is positioned parallel to the laminate at a distance of 5 mm, analogous to the simulation. The laminate is fixed vertically in a clamping device as shown in Figure 9.
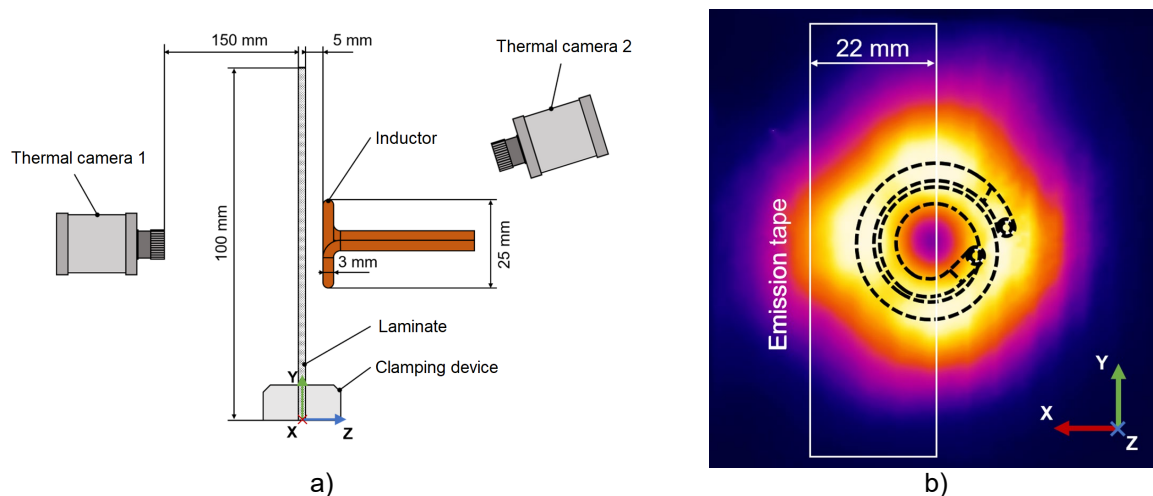

Fig.9: *Overview of the experimental setup of the validation tests a) (side view) and b) positioning of the emission tape using the example of the back of the laminate relative to the contour of the inductor located on the opposite side of the laminate (Thermal camera 1 view).*

The laminate is covered on both sides with an adhesive emission tape to assure the correct specification of the hemispherical emissivity. Furthermore, the emissive tape has a more homogeneous structure compared to the laminate surface and thus leads to a smoothing of the measured contour plots. The emission tape covers only one half of the zone influenced by the inductor (see Figure 9). The setup of the heating tests is identical to that of the model created in section 3.1. As the laminate is clamped vertically, the calculated convection coefficients for the case of vertical convection are used.

4.1.2 Comparison of the validation tests and simulation

In addition to the heating pattern, the heating rates of the test and simulation are also compared. In order to validate the FE model, two different methods of viewing the results are used. The qualitative comparison of test and simulation takes place via the observation of the heating curves. For this purpose, the maximum temperatures within the measuring fields on the front and back of the laminates are measured over time during the heating process. The location of the maximum temperature along with the heating rate of the simulated laminate is also determined.

The second method of validation is the qualitative evaluation of the heating pattern. For this purpose, the heating pattern on the side of the laminate facing away from the inductor is observed. An assessment of the heating pattern on the front side of the laminate is only possible to a limited extent as the inductor obstructs the view of the laminate. The laminates introduced in section 2 are used for the validation tests. The validation tests are carried out with four test specimens for each FVC. The heating curves of these four specimens are then averaged in each case. The layer structure of the FE model corresponds to those of the respective laminates. The parameters used in simulation and heating experiments are summarized below in Table 6.

Parameter	Simulation	Heating test
Generator power	-	40 %
f in KHz	490	≈ 490
V_f in %	32, 47, 60	32, 47, 60
t_{Lam} in mm	2.2, 2.0 and 2.5	2.2, 2.0 and 2.5
Layer configuration	$(-45/+45)_6 (-45/+45)_9 (-45/+45)_{12}$	NCF 6, 9 and 12 layers
$\hat{I}$ in A	297.5	-
Stop criteria	Maximum temperature 180°C	Maximum temperature 180°C

Table 6: Overview of the parameters used in the heating simulations and physical experiments for validation purposes

Comparing the heating curves of the simulation and validation tests on the front and back of the laminates, the following statements can be made for the laminates considered:

NCF 32%
- The magnitude of the heating curves of the simulation at the front and back of the laminate is far below the magnitude of the validation tests (see Figure 10).
- The temperatures at the front and back of the simulated laminate are close to each other. This can also be observed in the experimental validation tests.
- All curves show an initial flat region which can be seen in the first 0.1 seconds of heating.
- Typical rectangular heating patterns are formed in both the experiment and simulation. These heating patterns show the course of the currents in the 0° and 90° directions with distinct hotspots at the edges. The heating patterns of the simulation and validation tests agree qualitatively quite well.
- The temperatures reached in the contour plots of the simulated laminates are all below those of the tests. This is due to the fact that the heating rate at the back of the laminates calculated in the simulations is below that of the tests. This must be taken into account when qualitatively comparing simulation and tests.
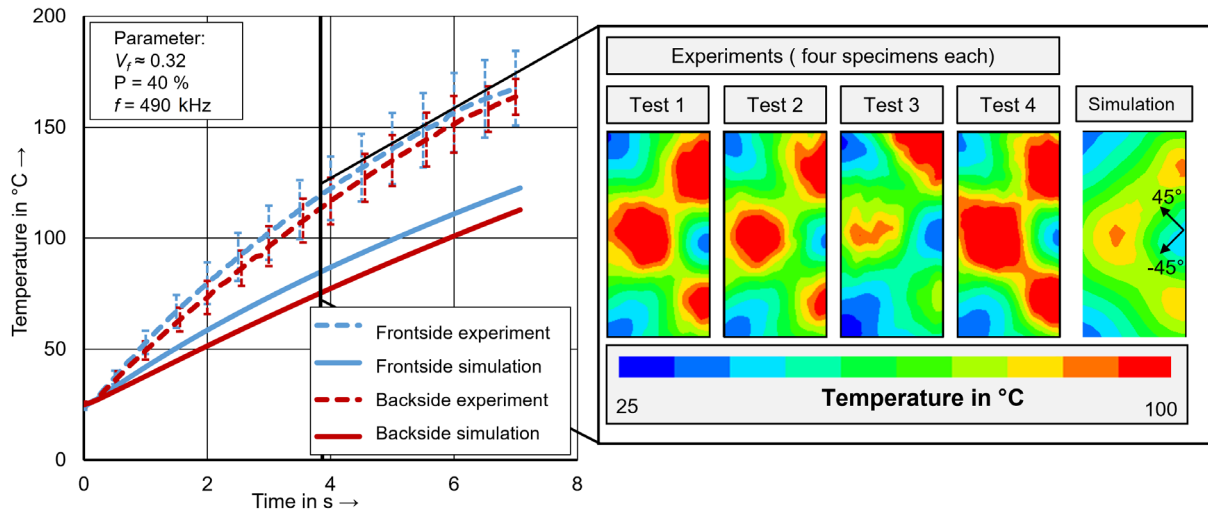
Fig.10: Comparison of simulation and experimental heating curves at front and back side of NCF-32% laminate (left) and heating patterns on back side at t = 3.9s.

NCF 47%

- The nature of the heating curves in the simulation at the front and back of the laminate agree very well with those of the tests, both qualitatively and quantitatively and are only slightly below that of the experimental validation tests (see Figure 11).
- All curves show an initial flat region which can be seen in the first 0.1 seconds of heating.
- Typical rectangular heating patterns are formed in the experiment and simulation. These heating patterns show the pathway of the currents in the 0° and 90° directions. The heating patterns of the simulation and validation tests agree qualitatively very well.
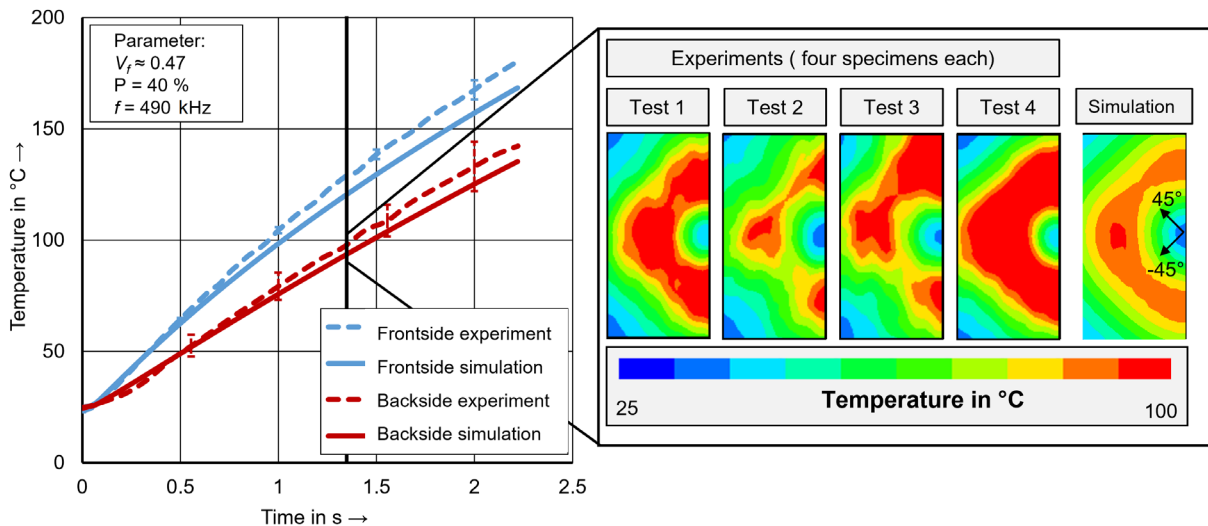

Fig.11: Comparison of simulation and experimental heating curves at front and back side of NCF-47% laminate (left) and heating patterns on back side at t = 1.3 s.

NCF 60%

- The nature of the heating curves in the simulation at the front and back of the laminate agree quantitatively very well with those of the experimental validation tests and fall only slightly below the experimental curves (see Figure 12). On the top side of the laminate, the deviation of the temperature in the simulation from the heating test is less than 5%.
- All curves again show an initial flat region, which can be seen in the first 0.1 seconds of heating.

- With higher FVCs, the heating pattern takes on a circular shape corresponding to the geometry of the induction coil and the hotspots are no longer recognizable. The heating patterns of the simulation and validation tests agree qualitatively very well.
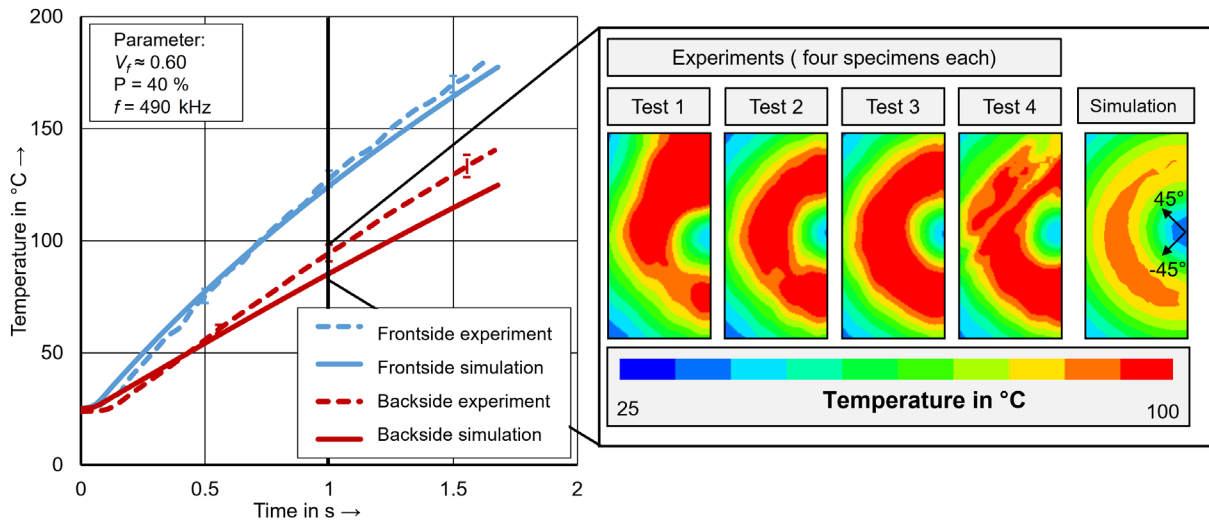

Fig.12: Comparison of simulation and experimental heating curves at front and back side of NCF-60% laminate (left) and heating patterns on back side at t = 1 s.

4.2 General statements on the results of the simulation

The results presented so far in section 4.1 are all reproducible with conventional characterization tests. However, a major advantage of FEA is the possibility to visualize quantities which are difficult or even impossible to measure experimentally. The findings obtained from the evaluation of these quantities are presented in this section. The considered quantities are obtained from the simulation results of the NCF 47% laminate presented in section 4.1 (see Table 7).

Parameter	Value
$\hat{I}$ in A	297.5
f in KHz	490
V_f in %	47
t_{LAM} in mm	2.3
Layer configuration	$(-45/+45)_{10}$
Stop criteria	Maximum temperature 180°C

Table 7: Simulation parameters used for the general investigation of the heating behavior.

4.2.1 Through thickness temperature distribution in the laminate

The first quantity considered in this section is the temperature profile in the thickness direction of the laminate. This quantity is difficult to measure experimentally. One approach found in the literature is to embed thermocouples between the individual layers of the laminate as carried out by Schieler et. al. [15]. The measured curves show the same characteristic curve as can be seen in the simulation results (see Figure 13). However, a direct comparison is not possible due to the different materials and test parameters, which have been used. The temperature curve in the thickness direction resulting from the simulation has its maximum temperature 0.23 mm below the surface of the laminate. The maximum temperature therefore occurs exactly between the second and third layers of the laminate used here. The temperature curve then flattens out again close to the rear surface of the laminate.
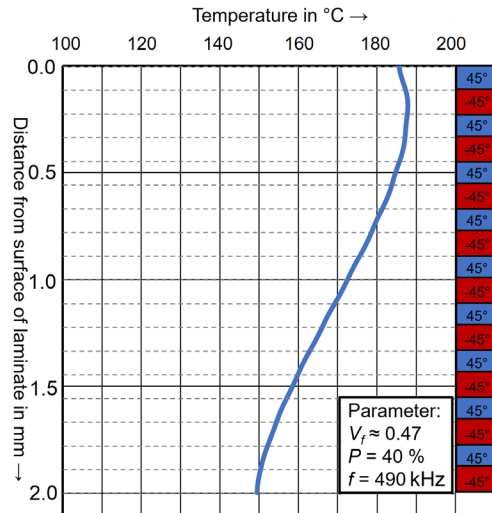
Fig.13: Temperature curve in thickness direction of the laminate at the point of maximum temperature development. The thickness of the laminate is 2.3 mm.

The characteristic shape of the temperature curve in the thickness direction described in this section can be justified as follows:

- The general shape of the curve can be explained by the distribution of the magnetic field in the laminate. The strength of the magnetic field decreases in the direction moving towards the back of the laminate.
- The maximum temperature occurring in the simulation is found to be between the upper two layers. On the one hand, this can be caused by the cooling of the surface by free convection. Furthermore, it can be assumed that the heat development mainly occurs near the boundary between two layers.
- The flattening of the temperature towards the back of the laminate can be explained by the heat conduction through the laminate in the thickness direction. The heat in the deeper layers of the laminate migrates towards the cooler rear side of the laminate. This leads to the diffusion of the temperature in the thickness direction and therefore to the recognizable flattening behavior.

4.2.2 Distribution of electric current density in the laminate

Another parameter that cannot be measured directly in experimental tests is the distribution of the electric current density in the laminate. The observation of the electric current density can give further information regarding the different heating mechanisms, which occur in the laminate. In particular, the behavior of the current at the roving crossover regions can be examined in more detail.

In this section, two areas are defined for the investigation of the distribution of the electric current density within the laminate. The first region (**Area A**) is representative of the four intersection areas where increased heat generation can be seen (see Figure 14). The second region (**Area B**) represents the four areas between the crossover areas where a lower heat generation is observed. In addition to the representation of the current density in the laminate via colored area contour plots in Figure 14, a further representation method for the current density is introduced. For this purpose, analogous to the visualization of the temperature curve in the thickness direction of the laminate, a curve describing the magnitude of the electric current density in the thickness direction is shown (see Figure 15). Here, a distinction is also made between **Area A** (see Figure 15 a)) and **Area B** (see Figure 15 b)). The following statements (considering first **Area B** for clarity of discussion) can be made for the two areas on the basis of the selected representation methods:

Area B

- A large part of the current runs in this area only in every second layer. Depending on the orientation of the laminate to the coil, these are either 90° layers or the 0° layers. Conversely, this means that the heating in this area occurs predominantly in every second UD-layer.
- Within the strongly current-carrying UD-layers, a pattern of the current density progression in the thickness direction can be seen. The current distribution within a UD-layer is not homogeneous but is concentrated in the areas close to the neighboring layers.

- This pattern is not visible in the layers close to the surfaces of the laminate. There, the current density is concentrated in the middle of the UD-layer.
- The maxima occurring in the layers with strong current flow show a course similar to the shape of the temperature distribution in the thickness direction.

Area A
- In this area, the current is distributed much more homogeneously over the entire thickness of the laminate. The differences in the electrical current density between the +45° and -45° layers are relatively small here
- The pattern of the variation of the electric current density in the thickness direction (for individual layers (each represented by 3 elements)) observed in **Area B** is also found in this region, albeit in a much weakened form.
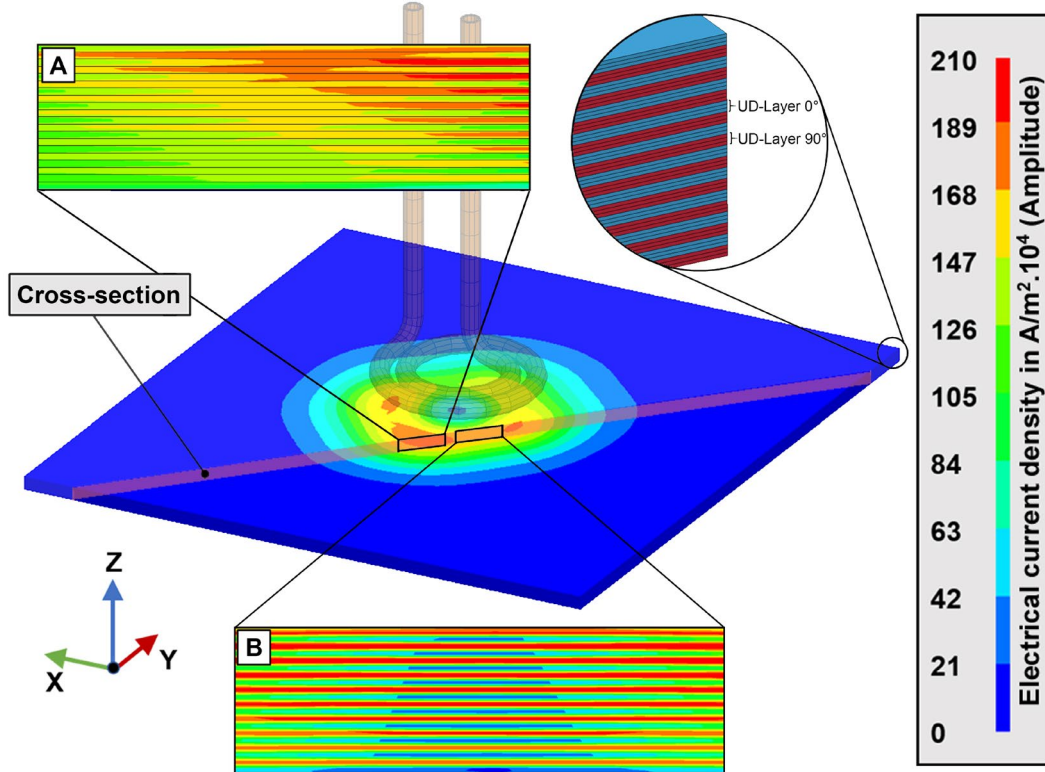

*Fig.14: Distribution of current density at different locations of the laminate: **A** at crossover areas; **B** between crossover areas.*
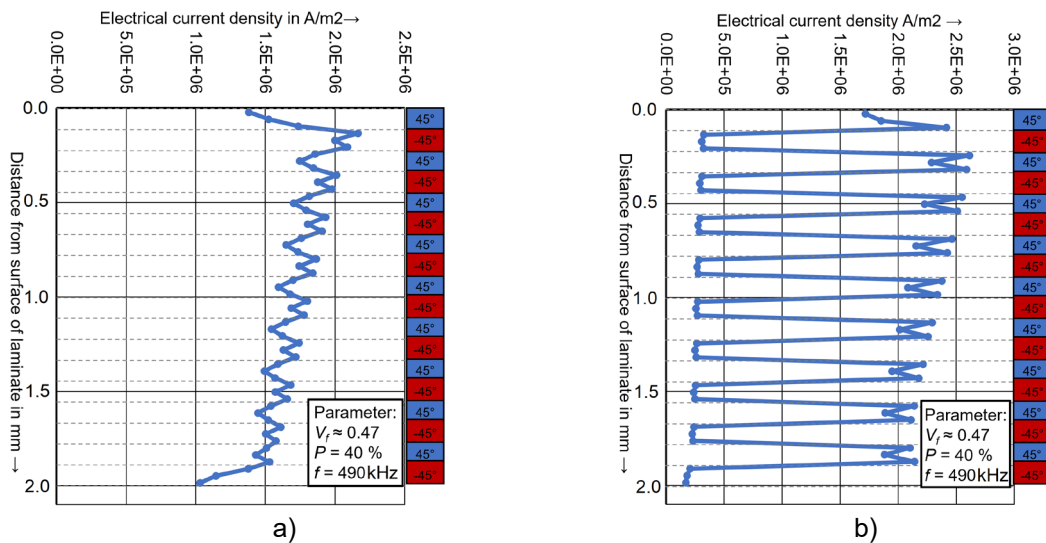

*Fig.15: Course of the current density in the thickness direction of the laminate between the crossover areas (a), area **A**, Figure 14) and at the point of maximal heating (b), area **B**, Figure 14).*

4.3 Influence of the layer orientation

Previous FE models for the inductive heating of CFRTPC laminates at the IVW were limited to macro-level isotropic material models. Models of this type are not able to represent the influence of the alignment of the individual layers. With the material model created in this work, this influence can be investigated directly. The alignment of the individual UD-layers to each other not only has an influence on the heating rate, but also on the resulting heating pattern. With an angular difference of 0° between the UD-layers in the laminate, i.e. a purely unidirectional structure, there is practically no heating of the laminate. In this section, we will investigate how the angle difference of the individual plies qualitatively and quantitatively affects the heating behavior of a laminate. To investigate the influence of ply orientation, the angular difference of the plies is changed in 10° steps from $(0/90)_{10}$ to $(0/50)_{10}$ (see Figure 16). Laminate set-ups with angle differences below 50° do not lead to any convergence with the version of the LS-DYNA® solver used in this work. For this study, the parameters listed in Table 8 were used.
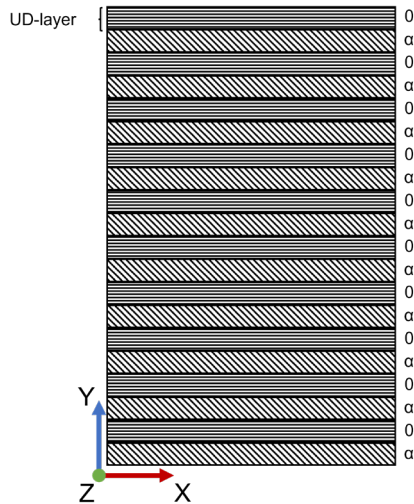

Fig.16: Schematic representation of the layer structures used for the investigation of the influence of the layer orientation on the laminate heating behavior.

Parameter	Value
$\hat{I}$ in A	297.5
f in MHz	490
V_f	0.5
t_{LAM} in mm	2
Layer configuration	$(0/90)_{10}$, $(0/+80)_{10}$, $(0/+70)_{10}$, $(0/+60)_{10}$, $(0/+50)_{10}$,
Stop criteria	Simulation time 5 sec

Table 8: Simulation parameters used for the investigation of the influence of ply orientation.

Looking at the heating behavior resulting from the different ply orientations as given in Figure 17, the following statements can be made:
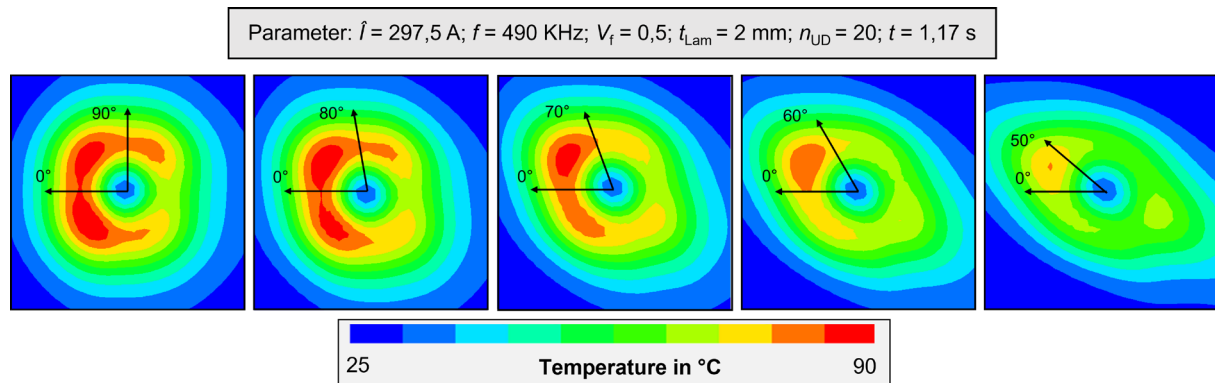

Fig.17: Influence of ply orientation in the laminate on the resulting heating pattern on the backside of the laminate.

- If the resulting heating patterns are compared as a color area contour plot, a clear influence of the ply orientation on the qualitative heating behavior becomes apparent (see Figure 17). The heating pattern becomes more and more diamond-shaped from its almost square shape with decreasing angle difference between the individual layers.
- Furthermore, the intensity of the resulting hotspots is reduced with decreasing angle difference and the temperature profile on the laminate surface appears more homogeneous.
- If the heating rates of the different simulations are compared, there is a clear correlation between the angle difference of the individual layers and the heating rate. The heating rate decreases with decreasing angle difference between the individual layers.

5 Summary and outlook

The objective of this work was to implement an analytical model describing the inductive heating behavior of textile-reinforced carbon fiber organic sheets in an FEM model for the thermal simulation of the static induction heating process. For this purpose, the electromagnetic solver in LS-DYNA® was chosen based on its advanced simulation capabilities. A meso-level material model was created using material parameters largely determined by micromechanical considerations. In order to further increase the accuracy of the FEM model, DSC measurements were carried out to determine the temperature dependence of the heat capacity of the laminates used. The material model was then integrated into an induction heating simulation model in LS-DYNA®. The model was validated for NCF laminates with FVCs of 32 %, 47 % and 60 % via heating tests. In general, the tests could be approximated well both quantitatively and qualitatively. The current work has built on and extended the existing isotropic FE models developed for continuous induction welding simulation at the IVW. Future possible extensions include full part-level simulations of aircraft CFRTPC structures involving complex UD-laminate configurations with reduced material characterization and validation requirements.

6 Acknowledgment

7 Literature

[1]   Ahmed T. J, Stavrov D, Bersee H.E.N, Beukers A. "Induction welding of thermoplastic composites—an overview", Compos. Part A Appl. Sci. Manuf., 37 (2006), pp. 1638-1651. https://doi.org/10.1016/j.compositesa.2005.10.009

[2]   Yarlagadda, S., Kim, H. J., Gillespie, J. W., Shevchenko, N. B. and Fink, B. K. "A Study on the Induction Heating of Conductive Fiber Reinforced Composites", J. Compos. Mater., Vol.: 36 Issue: 4, (2002) pp. 401-421. https://doi.org/10.1177/0021998302036004171

[3]   Kim, H. J., et. al. "Development of a Numerical Model to Predict In-plane Heat Generation Patterns During Induction Processing of Carbon Fiber-reinforced Prepreg Stacks", J. Compos. Mater., Vol.: 37 Issue: 16, (2003) pp. 1461-1483. https://doi.org/10.1177/0021998303034460

[4]   Fink, B. K, McCullough, R. L, Gillespie, J. W. "Experimental verification of models for induction heating of continuous-carbon-fiber composites", Polym. Composite, Vol.:17, (1996), pp.198–209. https://doi.org/10.1002/pc.10605

[5]   Senghor, F. D. et. al, "Electrical Conductivity Tensor Modeling of Stratified Woven-Fabric Carbon Fiber Reinforced Polymer Composite Materials", in IEEE Transactions on Magnetics, vol. 53, no. 6, pp. 1-4, 2017, https://doi.org/10.1109/TMAG.2017.2660529

[6]   Wasselynck, G., Trichet, D., and Fouladgar, J. "Determination of the Electrical Conductivity Tensor of a CFRP Composite Using a 3-D Percolation Model", in IEEE Transactions on Magnetics, vol. 49, no. 5, pp. 1825-1828, May 2013, https://doi.org/10.1109/TMAG.2013.2241039

[7]   Schürmann, H. "Konstruieren mit Faser-Kunstoff-Verbunden", Darmstadt: Springer Verlag, 2007. ISBN 978-3-540-72190-1

[8]   Lundström, F., Frogner, K., Andersson, M. "A numerical model to analyse the temperature distribution in cross-ply CFRP during induction heating", Composites Part B, Vol.: 202, (2020), 108419. https://doi.org/10.1016/j.compositesb.2020.108419

[9]   Isabellenhütte Heusler GmbH & Co. KG, "Isabellenhütte", [Online]. Available: https://www.isabellenhuette.de/fileadmin/Daten/Praezisionslegierungen/Datenblaetter_Widerstand/E_KUPFER.pdf [accessed on 06.10.2020].

[10]   BASF,   "Campusplastics",   [Online].   Available: https://www.campusplastics.com/campus/de/datasheet/Ultramid%C2%AE+A4H/BASF/20/fbec0c52 [accessed on 01.01.2020].

[11]   Duhovic M., Moser L., Mitschang P., Maier M., Caldichoury I., L'Eplattenier P. Simulating the Joining of Composite Materials by Electromagnetic Induction. In Proceedings of the 12th International LS-DYNA® Users Conference, Electromagnetic (2), 3.-5. June, 2012, Detroit, USA. https://www.dynalook.com/conferences/12th-international-ls-dyna-conference/electromagnetic16-c.pdf

[12]   Duhovic M., Hümbert M., Mitschang P., Maier M., L'Eplattenier P., Caldichoury I. Further Advances in Simulating the Processing of Composite Materials by Electromagnetic Induction. In: Proceedings of the 13th International LS-DYNA® Users Conference, Electromagnetic, 8.-10. June, 2014, Detroit, USA. https://www.dynalook.com/conferences/13th-international-ls-dyna-conference/electromagnetic/further-advances-in-simulating-the-processing-of-composite-materials-by-electromagnetic-induction

[13]   Duhovic M., L'Eplattenier P., Caldichoury I., Mitschang P., Maier M. Advanced 3D Finite Element Simulation of Thermoplastic Carbon Fiber Composite Induction Welding. ECCM16 - 16th European Conference on Composite Materials, 22.-26. June, 2014, Seville, Spain. http://www.escm.eu.org/eccm16/assets/0346.pdf

[14]   Duhovic M., Hausmann J., L'Eplattenier P., Caldichoury I. A Finite Element Investigation into the Continuous Induction Welding of Dissimilar Material Joints. In: Proceedings of the 10th European LS-DYNA® Users Conference, Process VII – Welding, 15.-17. June, 2015, Würzburg, Germany. https://www.dynalook.com/conferences/10th-european-ls-dyna-conference/3%20Process%20VII%20-%20Welding/02-Duhovic-InstitutfuerVerbundwerkstoffe-P.pdf/view

[15]   Schieler, O., Beier, U., and Mitschang, P. "Control of the through-thickness temperature distribution in carbon composite aerospace parts during induction welding", J. Thermoplast. Compos. Mater. Vol.: 31 Issue: 12, (2018) pp. 1587-1608. https://doi.org/10.1177/0892705717738390